Chinese Journal of Aeronautics, (2013),26(6): 1449–1458

Chinese Society of Aeronautics and Astronautics
& Beihang University

Chinese Journal of Aeronautics

cja@buaa.edu.cn
www.sciencedirect.com

Thermal-structural response and low-cycle fatigue damage of channel wall nozzle

Cheng Cheng, Wang Yibai *, Liu Yu, Liu Dawei, Lu Xingyu

School of Astronautics, Beihang University, Beijing 100191, China

Received 28 March 2013; revised 24 May 2013; accepted 22 July 2013
Available online 2 August 2013

KEYWORDS

Channel wall nozzle;
Damage;
Life;
Low-cycle fatigue;
Reusable engine;
Thermal-structural response

Abstract To investigate the thermo-mechanical response of channel wall nozzle under cyclic working loads, the finite volume fluid-thermal coupling calculation method and the finite element thermal-structural coupling analysis technique are applied. In combination with the material low-cycle fatigue behavior, the modified continuous damage model on the basics of local strain approach is adopted to analyze the fatigue damage distribution and accumulation with increasing nozzle work cycles. Simulation results have shown that the variation of the non-uniform temperature distribution of channel wall nozzle during cyclic work plays a significant role in the thermal-structural response by altering the material properties; the thermal–mechanical loads interaction results in serious deformation mainly in the front region of slotted liner. In particular, the maximal cyclic strains appear in the intersecting regions of liner gas side wall and symmetric planes of channel and rib, where the fatigue failure takes place initially; with the increase in nozzle work cycles, the residual plastic strain accumulates linearly, and the strain amplitude and increment in each work cycle are separately equal, but the fatigue damage grows up nonlinearly. As a result, a simplified nonlinear damage accumulation approach has been suggested to estimate the fatigue service life of channel wall nozzle. The predicted node life is obviously conservative to the Miner's life. In addition, several workable methods have also been proposed to improve the channel wall nozzle durability.

1. Introduction

The increasing requirements regarding performance, reliability and service life of cryogenic liquid rocket engines in combination with the pressing need for reduction of both production and operational cost have led to the birth of the idea of reusable space transportation systems.[1,2] As an indispensable part of high performance, reusable liquid rocket engine such as the space shuttle main engine (SSME)[3,4] and RD-0120,[5] the regenerative cooling nozzle has made some significant contribution to the successful development and application of the launch vehicles. Fint et al. [6] introduced a brazed, milled channel wall nozzle construction applied to SSME which is different from the current SSME tube wall nozzle, and indicated that nozzles with slotted liners provide a more robust and lower-cost alternative to the tube wall nozzles. Moreover, the concept for a typical channel wall nozzle is a

* Corresponding author. Tel.: +86 10 82316855.
E-mail addresses: ccheng.buaa@gmail.com (C. Cheng), wangyibai@buaa.edu.cn (Y. Wang), liuyu@buaa.edu.cn (Y. Liu), liudoudou.hi@163.com (D. Liu), luxingyu6566@163.com (X. Lu).

Peer review under responsibility of Editorial Committee of CJA.

Production and hosting by Elsevier

1000-9361 © 2013 Production and hosting by Elsevier Ltd. on behalf of CSAA & BUAA. Open access under CC BY-NC-ND license.
http://dx.doi.org/10.1016/j.cja.2013.07.045

relatively simple and elegant design solution with a significantly reduced part count compared with a tube wall nozzle. This ultimately results in better reliability and longer service life. During the cyclic operation of pre-cooling, start up, hot run, shut down, post-cooling and relaxation, the elastic–plastic deformation of channel wall nozzle induced by the synergy of high-speed hot gas and high-pressure cryogenic coolant results in residual strain, and subsequently accumulates to an extent that cracks initiate (i.e., failure occurs) in the cooling channels after numerous work cycles. Hence, the low-cycle fatigue (LCF)[7–9] is the primary service life limit factor of regenerative cooling channel wall nozzle.

Substantial progress has been made on the research of life prediction methods for cooling channels of reusable thrust chambers,[10–13] but almost all the analytical models are restricted to the simplified throat cross section. The more notable thing is that few investigations on the fatigue damage mechanism and life estimation approach of channel wall nozzle can be retrieved although there are respectable surveys on the coolant flow and heat transfer of cooling channels.[14,15] The load-bearing conditions of regenerative cooling nozzle are quite different from that of thrust chamber during a full operation cycle. Specifically speaking, the pressure and heat flux caused by hot gas are subordinate, while the coolant pressure plays a dominant role in the nozzle deformation. In addition, the coolant flow and heat transfer as well as the channel wall deformation present obvious three-dimensional characteristics attributing to the sharp variation of channel aspect ratio axially along the nozzle extension. In the present study, the finite volume fluid-thermal coupling calculation method, nonlinear finite element thermal-structural coupling analysis method and local strain method are adopted to investigate the thermal-structural response and low-cycle fatigue damage of three-dimensional, regenerative cooling channel wall nozzle under cyclic working loads. The method of whole-field discretization and solution is applied to the coupled fluid-thermal model by finite volume approach, and the heat transfer in solid domain is evaluated directly by energy equation. During coupled thermal-structural analysis, the calculated thermal load and the changed material properties with temperature are employed as the important affecting factors to the structural response analysis in finite element approach. The local strain method is primarily used to assess the crack initiation life for low-cycle fatigue failure induced by cyclic elastic–plastic deformation under perilous loading conditions. Meanwhile, several methods are also suggested for improving the channel wall durability and a simplified fatigue life prediction method is provided for the slotted liner.

2. Computational configuration

The simplified conical contour has been adopted for the regenerative cooling nozzle. The optimized cooling channels are applied to the channel wall nozzle reference to the subscale hot-firing test nozzle by Volvo Aero Corp.[16,17] The main operational and structural parameters of the channel wall nozzle are given in Table 1. The high thermal conductivity copper-based alloy NARloy-Z[18] is used for liner material and the high strength nickel-based alloy Inconel-718 is chosen for jacket material. Considering the simulation accuracy and computational capacity, only one uniform block depicted in Fig. 1(a) is chosen as the computation domain. The block is divided from the three-dimensional channel wall nozzle corresponding to each circularly symmetric rib. The domain includes gas zone, coolant zone, liner zone and jacket zone. The finite volume mesh for fluid-thermal coupling calculation and the finite element mesh for thermal-structural coupling analysis are demonstrated in Fig. 1(b) and (c), respectively. The multi-block abutting structured grid approach[19] is applied to the finite volume model. The computational domain is decomposed into five isolated blocks along the fluid–solid coupled surfaces, through which the continuous temperature and heat flux are satisfied as the coupling interface conditions. Subsequently, the finite difference schemes are used to generate the structured grid in each block. To improve the simulation accuracy of boundary layer flow and fluid–solid heat transfer, mesh refinement in the vicinity of the coupled surfaces is employed. The three-dimensional, eight-node solid element is adopted to dissociate the finite element model. It can be used not only for structural analysis as Solid 45, but also for thermal analysis as Solid 70 based on ANSYS Workbench. Meanwhile, ascribing to the interpolation method introduced to applying the interface conditions,[20] different grid layouts on fluid–solid coupled surfaces between the finite volume model and the finite element model have been employed here.

3. Methodology

According to the variations of pressure and thermal load of the channel wall nozzle, the numerical simulation is demarcated into four load steps[21,22] as listed in Table 2. We conduct the fluid-thermal coupling calculation among hot gas, solid wall and coolant, and obtain the interface conditions on fluid–solid coupled surfaces for the finite element model. Subsequently, the nonlinear thermal-structural coupling analysis is applied to solving the stress–strain response of slotted liner under cyclic thermal–mechanical loads based on the following assumptions:

Table 1 Main operational and structural parameters of channel wall nozzle.

Parameter	Value	Parameter	Value
Chamber pressure (MPa)	11	Nozzle extension area ratio	5:1–36:1
Propellent	LO2/LH2	Channel number	66
Mixture ratio	6.0	Liner thickness (mm)	0.8 (5:1)–1.1 (36:1)
Coolant operating pressure (MPa)	20	Channel width (mm)	1.92 (5:1)–6.39 (36:1)
Coolant mass flow (kg/s)	1.188	Channel height (mm)	1.5 (5:1)–2.0 (36:1)
Coolant initial temperature (K)	200	Rib width (mm)	0.8
Throat diameter (mm)	24.8	Jacket thickness (mm)	1.1

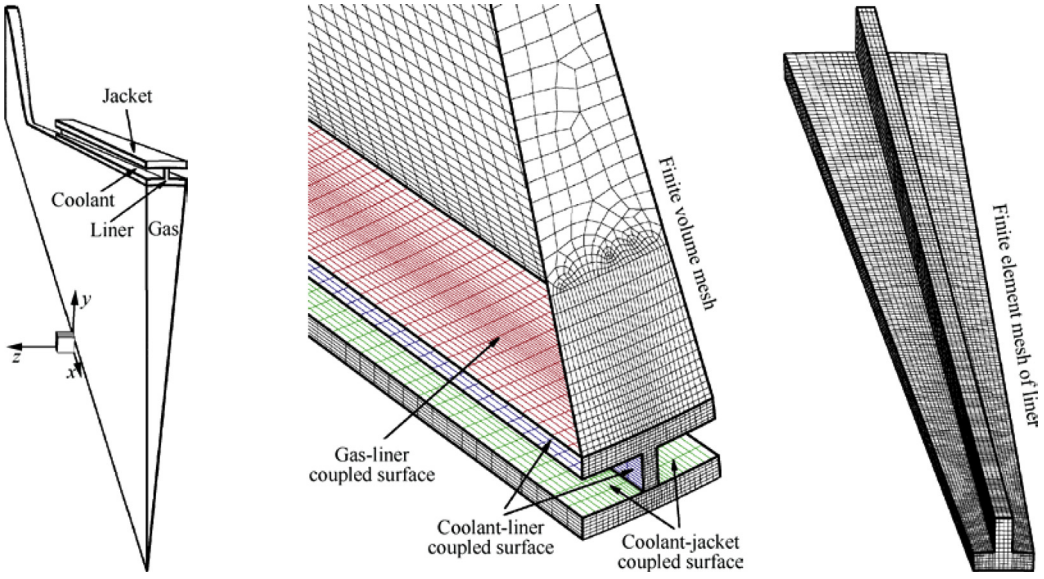

(a) Calculation model (b) Finite volume mesh (c) Finite element mesh

Fig. 1 Calculation model and mesh of channel wall nozzle.

Table 2 Calculation load steps of channel wall nozzle.

Load step	Operation stage	Coolant pressure (Mpa)	Assumed time (s)
I	Pre-cooling	0–15.6	22.5
II	Start up, hot run	15.6–20	190
III	Shut down, post-cooling	20–0	287.5
IV	Relaxation	0	100

(1) During the pre-cooling and post-cooling processes, the thermal field varies linearly between the uniform environmental temperature field and pre/post-cooling temperature field.
(2) With the pressure drop along cooling channels being ignored, the coolant pressure varies linearly during the cyclic operation. Moreover, the gas side wall pressure of nozzle extension is negligible.
(3) The elastic–plastic structural deformation of channel wall nozzle is not influenced by the progressing low-cycle fatigue damage.[23]
(4) The creep deformation of channel wall material is negligible.

The signed von Mises equivalent method is employed to acquire the cyclic strain amplitude for each finite element according to the "stretch" or "compress" status in the cyclic work process. In combination with the low-cycle fatigue behavior of nozzle materials, the local strain approach[24,25] is adopted to analyze the fatigue damage distribution of channel wall nozzle and the modified continuous damage model is applied to obtaining the damage accumulation feature with the increase of nozzle work cycles.

3.1. Fluid-thermal coupling calculation method

The complicated flow field of regenerative cooling nozzle, which includes supersonic, compressible hot gas and low-speed, incompressible cryogenic coolant, results in the Navier–Stokes equations with noticeable stiffness in numerical calculation. Hence, the time-derivative preconditioning method[26] is applied to adding time derivative of pressure to the continuity equations. The induced coupled pressure–velocity relation enhances the computational stability for incompressible flow, and yet has a negligible influence on the simulation convergence for supersonic flow. The preconditioned governing equations[27] can be written in vector notation as

$$\boldsymbol{\Gamma}\frac{\partial}{\partial t}\int_V \boldsymbol{Q}\mathrm{d}V + \oint [\boldsymbol{F} - \boldsymbol{F}_\mathrm{v}]\mathrm{d}A = \int_V \boldsymbol{H}\mathrm{d}V \tag{1}$$

where $\boldsymbol{\Gamma}$ is the preconditioning matrix; $\boldsymbol{Q}$, $\boldsymbol{F}$, $\boldsymbol{F}_\mathrm{v}$ and $\boldsymbol{H}$ are the vectors of primitive variables, convective variables, viscid variables and source variables, respectively. While $\boldsymbol{Q} = [p\ u\ v\ w\ T]^\mathrm{T}$, Eq. (1) can be used to calculate the flow behavior of hot gas and coolant as the simultaneous conservation equations of mass, momentum, and energy, where p, u, v, w and T are the pressure, component of velocity vector at x, y and z axes, and temperature, respectively; While $\boldsymbol{Q}$ is the internal energy $[E]$, Eq. (1) can simulate the thermal field of channel wall just as the function of temperature inside solid zone.

The calculations have been carried out by using the fully implicit finite volume method, and standard K–ε equations are applied for the turbulence model. To capture the flow features accurately, the discretization of the convective terms are done by the second-order upwind scheme and the viscid terms by the central difference scheme. Assumed to be idea gas, the thermodynamic parameters of hot gas are given in Table 3, where $\overline{M}$ is the mean molar mass, C_p is the specific heat at constant pressure, λ is the thermal conductivity, μ is the dynamic

Table 3 Thermodynamics parameters of hot gas (idea gas).

Parameter	Value
$\overline{M}$ (kg/kmol)	13.505
C_p (J/(kg·K))	8267.643
λ (W/(m·K))	0.6064
μ (kg/(m·s))	9.74×10^{-5}

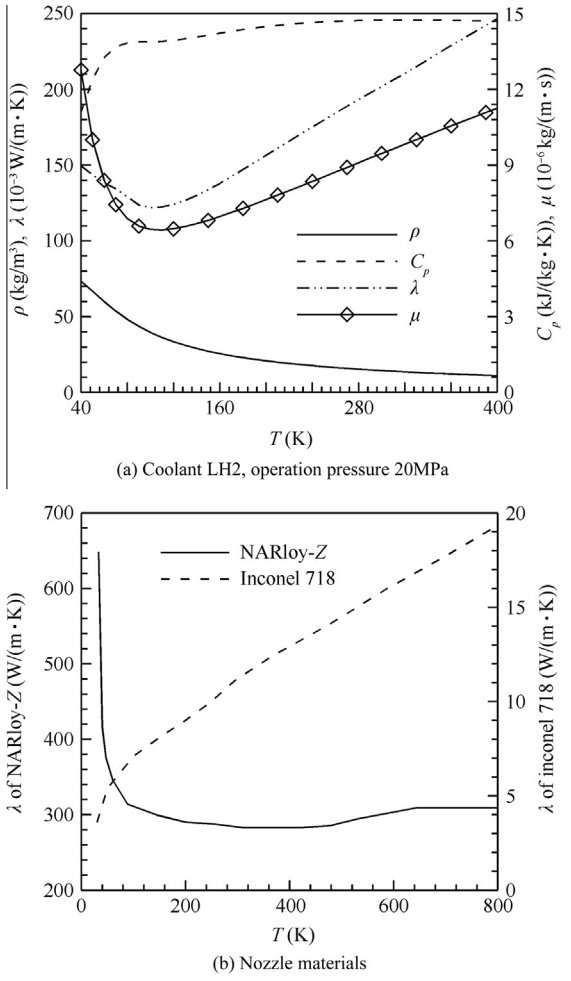

Fig. 2 Variation curves of thermodynamics parameters of coolant and nozzle materials vs temperature.

viscosity coefficient. The variation curves of coolant thermodynamic parameters with temperature under operation pressure 20 MPa are shown in Fig. 2(a) and the variation curves of thermal conductivity vs temperature for liner and jacket material are depicted in Fig. 2(b).

3.2. Thermal-structural coupling analysis method

Considering the variations in material thermodynamics properties with operational temperature, the equilibrium equation for nonlinear finite element thermal analysis of channel wall nozzle is described as

$$\boldsymbol{C}(\boldsymbol{T})\frac{\partial \boldsymbol{T}}{\partial t}+\boldsymbol{K}(\boldsymbol{T})\boldsymbol{T}=\boldsymbol{P} \tag{2}$$

where $\boldsymbol{C}(\boldsymbol{T})$ and $\boldsymbol{K}(\boldsymbol{T})$ are the matrixes of specific heat and thermal conductivity respectively; $\boldsymbol{T}$ and $\boldsymbol{P}$ are the vectors of node temperature and node heat flux respectively. The Galerkin weighted residual method[28] is used to solve the Fourier thermal conduction differential equation. The thermal boundary load is gradually applied by the automatic time steps. The Newton–Raphson method[29] is adopted to obtain the iterative solution of Eq. (2).

The cyclic thermal–mechanical loads interaction of channel wall nozzle usually leads to the elastic–plastic deformation. On the account of the nonlinear material constitutive relation, the static equilibrium equation for finite element thermal-structural coupling analysis is given as

$$\boldsymbol{K}_{\boldsymbol{T}}(\boldsymbol{\delta})\boldsymbol{\delta}=\boldsymbol{R}+\boldsymbol{R}^{\mathrm{th}} \tag{3}$$

where $\boldsymbol{K}_{\boldsymbol{T}}(\boldsymbol{\delta})$ is the global tangent stiffness matrix; $\boldsymbol{\delta}$, $\boldsymbol{R}$ and $\boldsymbol{R}^{\mathrm{th}}$ are the vectors of node displacement, node mechanical load and node thermal load, respectively. Because the stress is closely related to the loading history during the elastic–plastic deformation stage, the Euler-Newton method[30] has been applied to solving Eq. (3). Based on the incremental theory, the nonlinear constitutive equation during the loading process, where the plastic strain is characterized by von Mises yield criterion and isotropic hardening hypothesis,[21,31] is given as

$$\begin{cases} \mathrm{d}\boldsymbol{\varepsilon}=\mathrm{d}\boldsymbol{\varepsilon}^{\mathrm{e}}+\mathrm{d}\boldsymbol{\varepsilon}^{\mathrm{p}}+\mathrm{d}\boldsymbol{\varepsilon}^{\mathrm{th}} \\ \mathrm{d}\boldsymbol{\varepsilon}^{\mathrm{e}}+\mathrm{d}\boldsymbol{\varepsilon}^{\mathrm{p}}=\boldsymbol{D}^{-1}\mathrm{d}\boldsymbol{\sigma}+\frac{1}{A}\cdot\frac{\partial f}{\partial\boldsymbol{\sigma}}\left(\frac{\partial f}{\partial\boldsymbol{\sigma}}\right)^{\mathrm{T}}\mathrm{d}\boldsymbol{\sigma} \\ A=-\left(B+\left(\frac{\partial f}{\partial\boldsymbol{\sigma}^{\mathrm{p}}}\right)^{\mathrm{T}}\boldsymbol{D}\frac{\partial f}{\partial\boldsymbol{\sigma}}\right) \\ B=\frac{\partial f}{\partial\kappa}\boldsymbol{\sigma}^{\mathrm{T}}\frac{\partial f}{\partial\boldsymbol{\sigma}}\left(\kappa=w^{\mathrm{p}}\right) \end{cases} \tag{4}$$

where $\boldsymbol{\varepsilon}$, $\boldsymbol{\varepsilon}^{\mathrm{e}}$, $\boldsymbol{\varepsilon}^{\mathrm{p}}$, $\boldsymbol{\varepsilon}^{\mathrm{th}}$, $\boldsymbol{\sigma}$ and $\boldsymbol{\sigma}^{\mathrm{p}}$ are the vectors of node total strain, node elastic strain, node plastic strain, node thermal strain, node total stress and node plastic stress, respectively; $\boldsymbol{D}$ is the elastic matrix; $f=f(\boldsymbol{\sigma},\kappa)$ is the loading function with κ being the strengthen parameter reflecting the load history and w^{p} being the plastic work. The stress–strain behavior at different operational temperatures of liner material[32] is shown in Fig. 3. It reveals that the thermal load can not only bring about the channel wall deformation directly, but also affect the structural response by influencing the material constitutive relation as well.

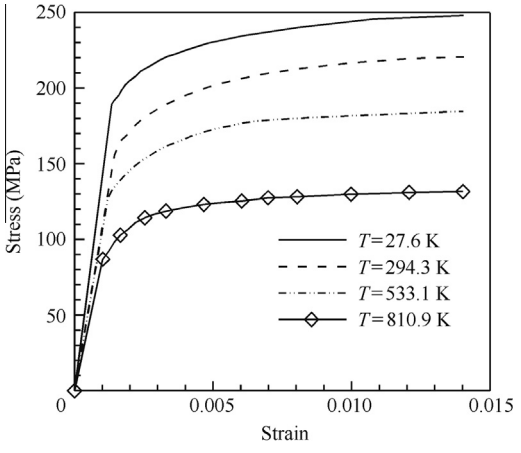

Fig. 3 Stress–strain curves of liner material at different operation temperatures.

3.3. Low-cycle fatigue damage calculation method

Several models have been proposed to determine the number of cycles to failure based on stress, strain, or energy. The stress-based approach, which is the oldest method to life prediction, is usually expressed as a function of the fatigue strength parameters. Basquin[33] proposed the equation as follows:

$$\sigma_a = \sigma'_f (2N_f)^b \tag{5}$$

where σ_a, N_f, σ'_f and b are the cyclic stress amplitude, fatigue life, fatigue strength coefficient and fatigue strength exponent, respectively. Power-law equation is the most common type for the stress-based fatigue life models.

The strain-based approach, which is one of the most widely used methods for predicting the material life, is especially useful in the case of low-cycle fatigue. If only plastic strain is considered, the function correlating the number of cycles to plastic strain is described by the Coffin–Manson[34] equation as

$$\frac{\Delta\varepsilon_p}{2} = \varepsilon'_f (2N_f)^c \tag{6}$$

where $\Delta\varepsilon_p$, ε'_f and c are the inelastic strain range, fatigue ductility coefficient and fatigue ductility exponent, respectively.

Based on Miner's rule of linear damage accumulation,[35] the low-cycle fatigue life is provided by the Basquin and Coffin-Manson equations. Employing the mean stress correction,[36,37] the calculation formula is given as follows:

$$\varepsilon_a = \frac{\sigma'_f - \sigma_m}{E}(2N_f)^b + \varepsilon'_f \left(1 - \frac{\sigma_m}{\sigma'_f}\right)^{(c/b)} (2N_f)^c \tag{7}$$

where ε_a, σ_m and E are the cyclic strain amplitude, mean stress and elastic modulus, respectively. As shown in Fig. 4, the cyclic strain-life curves of channel wall materials are mostly derived by the Manson universal slope method.[38]

In the damage theory, the fatigue damage is usually described by the remaining life, which is a major concept that can be best illustrated in Eq. (8). D is the damage after the initial damaging process, and N represents the current number of cycles already applied. Specifically, the fatigue damage D will be equal to 0 for the undamaged material and 1 at the time of rupture.

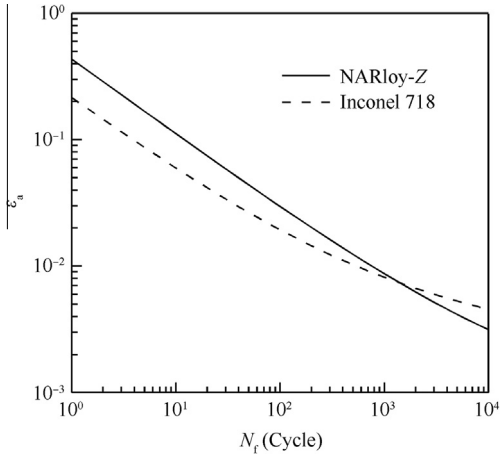

Fig. 4 Low-cycle fatigue behavior of channel wall material by Manson universal slope.

$$D = \frac{N}{N_f} \tag{8}$$

Since the channel wall nozzle is subject to loading spectrum of varying strain excursion for different work cycles under uniform constraint conditions, the modified continuous damage model[39] as depicted in Eq. (9) is proposed to evaluate the low-cycle fatigue damage D_n after n work cycles. On the basis of the assumption that the stress–strain behavior travels along the identical hysteresis loop within a work cycle, the cycle-based approach is applied to estimating the fatigue damage d_i for the ith work cycle, which is defined as the reciprocal of Miner's life $N_{f,i}$.

$$\begin{cases} D_n = \sum_{i=1}^{n} d_i \\ d_i = 1/N_{f,i} \end{cases} \tag{9}$$

Table 4 Grid independence validation of channel wall nozzle.

Model	Grid layout					Liner grid	
	a	*b*	*c*	*d*	*e*	Elements	Nodes
Case 1	1	3	2	3	100	1700	3030
Case 2	2	5	3	4	140	6160	9024
Case 3	3	8	5	6	180	20340	26064
Adopted mesh	4	10	6	8	200	35200	43215
Case 4	5	12	8	10	220	62040	72930

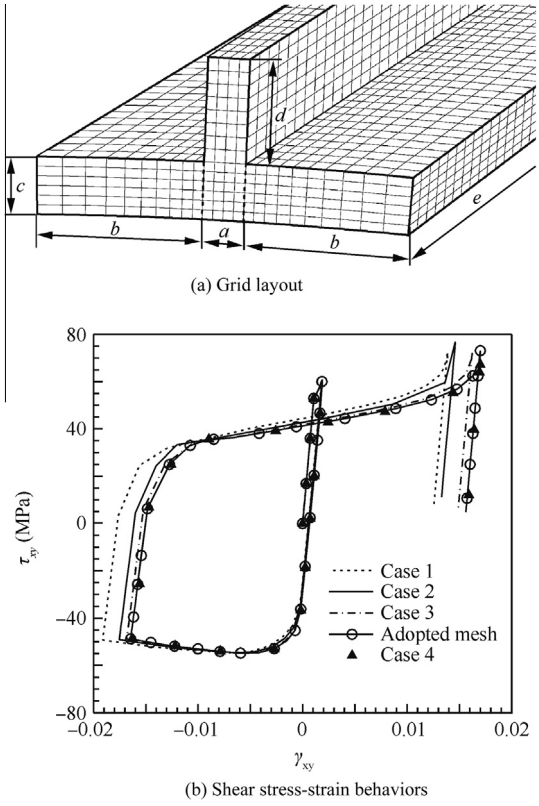

Fig. 5 Grid independence validation for thermal-structural response analysis.

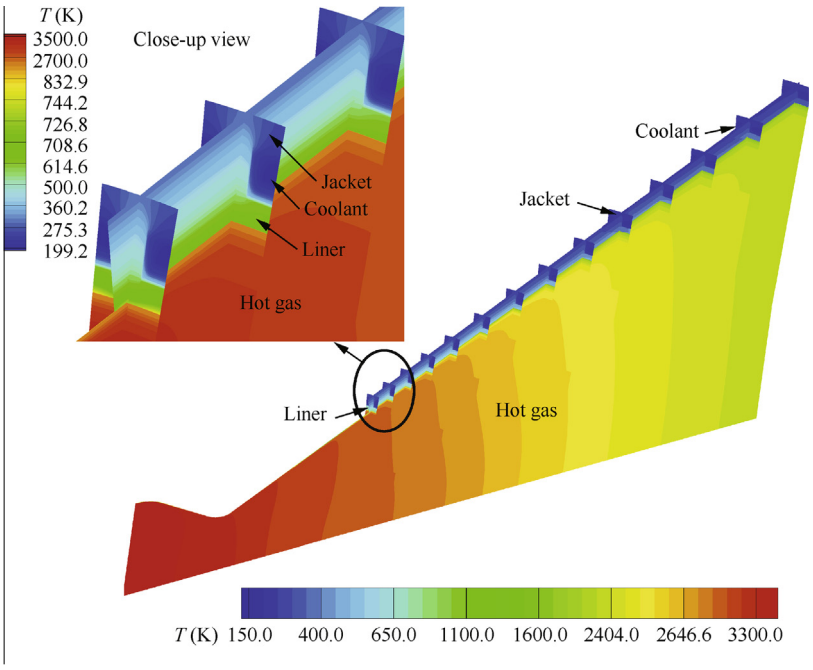

(a) Fluid-thermal coupled field

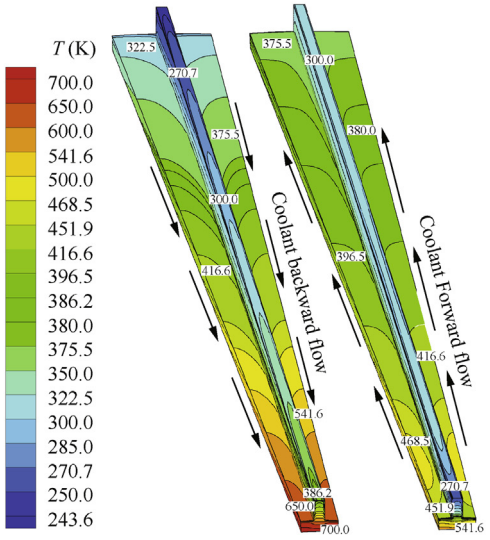

(b) Liner temperature

Fig. 6 Temperature distribution of channel wall nozzle during stationary work.

3.4. Grid independence validation

In view of the thermal-structural response of channel wall nozzle being the core part in the present context, calculations have been carried out by using different finite element meshes as given in Table 4. The explicit grid layout of slotted liner is illustrated in Fig. 5(a). The comparison of the node shear stress–strain behaviors in the identical location for different cases is shown in Fig. 5(b). Although the number of finite element nodes of Case 4 is much larger than that of the employed model, the difference of the thermo-mechanical results between the two models is inappreciable, whereas the difference between Case 3 and the employed model is slightly obvious. It is evident that the adopted mesh in this work is undoubtedly acceptable for adequate solution accuracy as well as admissible computational efficiency.

4. Results and discussion

4.1. Thermal load analysis

With coolant backward flow layout applied in this study, the temperature distribution of channel wall nozzle during hot run is presented in Fig. 6. In conjunction with the diminished temperature and pressure of hot gas in the nozzle extension,

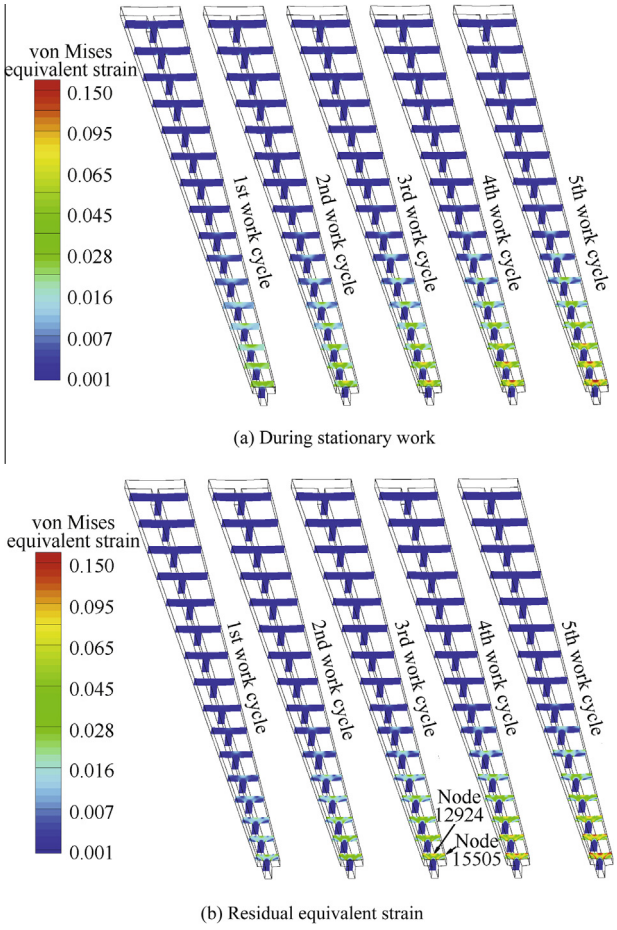

(a) During stationary work

(b) Residual equivalent strain

Fig. 7 Von Mises strain distribution of slotted liner with increasing work cycles.

the efficient regenerative cooling results in relatively lower thermal load distribution of the slotted liner. As shown in Fig. 6(b), the maximum temperature occurring at gas side wall of nozzle extension inlet is approximately 700 K, and the liner temperature close to nozzle outlet not exceeds 400 K. Since the material properties are sensitively affected by the thermal load as illustrated in Fig. 3, the strength of liner material at nozzle inlet is distinctly inferior to that at nozzle outlet. The channel structural strength, on the contrary, drops markedly with the increase in nozzle area ratio due to the unceasingly enlarged channel width. For this reason, appropriately attenuating the liner thickness at nozzle inlet for enhancing the heat transfer and increasing the liner thickness at nozzle outlet for heightening the structural reliability just as in this paper can effectively improve the channel wall robustness. On the other hand, the gradually dwindling channel height toward the nozzle inlet employed in this work has also brought the liner temperature down a little due to the further accelerated coolant flow. And if it is all right, adding the coolant mass flow and adopting the multi-section cooling concept will aggrandize the durability of channel wall nozzle incontestably. Another preferable way to lessen the thermal load of slotted liner is applying the coolant forward flow layout for channel wall nozzle. The temperature distributions of the two coolant flow layouts are compared in Fig. 6(b). Although the minimum temperature has a slight increase close to nozzle outlet, the maximum temperature of slotted liner falls visibly by about 160 K.

4.2. Thermal-structural response

The distributions of von Mises equivalent strain of channel wall nozzle during the cyclic working process are presented in Fig. 7. Owing to the somewhat severe thermal strain and the considerable plastic strain close to the nozzle extension inlet, which is caused by the integrated effect of the reduced material strength and the diminishing liner thickness, the appreciable channel wall deformation generally occurs in the front region of the slotted liner. The most serious strain is mainly located at the intersecting regions of liner gas side wall and symmetric planes of channel and rib, where the fatigue failure takes place initially. Another obvious feature given in Fig. 7 is that the equivalent strain of the slotted liner continuously rises with the increase in nozzle work cycles, especially noteworthy in the above dangerous regions. The substantial residual strain after each work cycle as shown in Fig. 7(b) also reveals that the plastic strain accumulation is the primary incentive for the fatigue failure of channel wall nozzle.

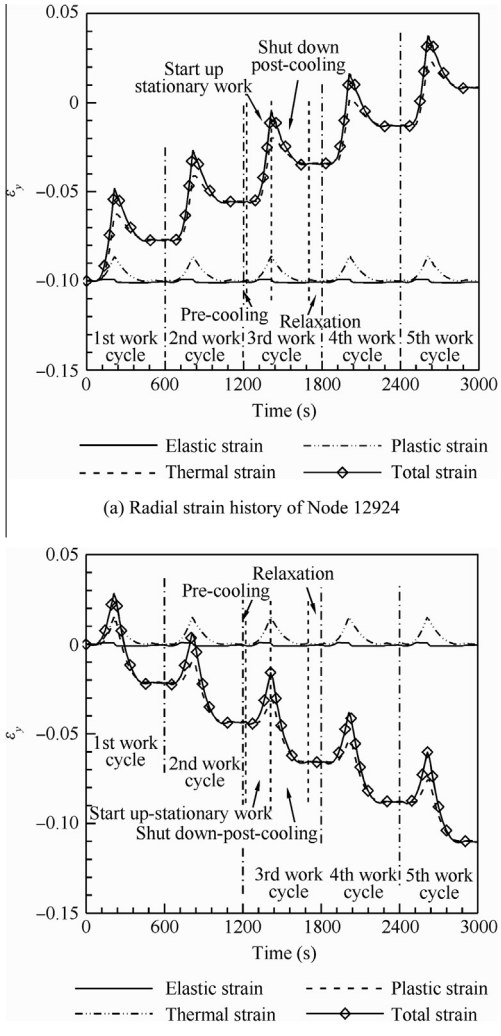

(a) Radial strain history of Node 12924

(b) Radial strain history of Node 15505

Fig. 8 Node strain history during cyclic work process.

For more intelligible analysis, the time histories of node radial strain (i.e. y component) are illustrated in Fig. 8. The representative nodes in the dangerous regions of channel wall nozzle are given in Fig. 7(b). The time history of the total node strain is primarily dominated by the variation of plastic strain, and the thermal strain also plays a significant role in it, but the contribution of elastic strain can be ignored. Since the typical Node 12924 and Node 15505 are located at the symmetric plane of rib and channel respectively, the forced states and deformation modes under the coolant pressure are conspicuously different. The plastic strains and total strains of the two nodes persistently accumulate in approximately opposite directions with the increasing work cycles of channel wall nozzle, whereas similar thermal strain variations are obtained due to their lying in the same axial cross section of slotted liner. The accumulation processes of node radial strains also reveal that the residual strains of Node 12924 and Node 15505 both approximately augment linearly with the increase in nozzle work cycles. And, furthermore, the strain growing ranges are remarkable.

Sequentially undergoing the cyclic operations, the essentially uniform strain variations in each work cycle for Node 12924 and Node 15505 can be obtained. In view of the plastic strain and thermal strain of Node 12924 varying in the same direction, the maximum node radial strain occurs during stationary work, while both of the plastic and thermal strains hit the maximal magnitude. Then, with the decrease of coolant pressure and thermal load, the total node strain reduces to the residual plastic strain. On the contrary, ascribing to the plastic strain and thermal strain of node 15505 varying in the opposite directions, the node radial strain during stationary work turns into the minimum in each work cycle, and the residual strain becomes the maximal magnitude.

The shear stress–strain responses of typical nodes in the dangerous regions of the slotted liner are shown in Fig. 9. It makes clear that the increasing work cycles lead to the stress–strain hysteresis loops of Node 12924 and Node 15505 developing in opposite directions. Though both the residual and mean shear strains of the two nodes grow up unceasingly during the cyclic working process, the strain amplitudes as well as the strain increments in each work cycle are almost equal. Consequently, this cyclic creep of channel wall nozzle under consistent thermo-mechanical restrictions is known as the ratcheting behavior.[22] Moreover, a close-up view of the detailed stress–strain behavior in the first work cycle is given in Fig. 9(b). With the variation of thermal load during the cyclic work, the altering material strength plays a dramatic role in the thermal-structural response of channel wall nozzle. Specifically speaking, the softening liner during hot run produces a drastic deformation under nearly invariable coolant pressure action, whereas the hardening material during post-cooling compels the plastic strain changes.

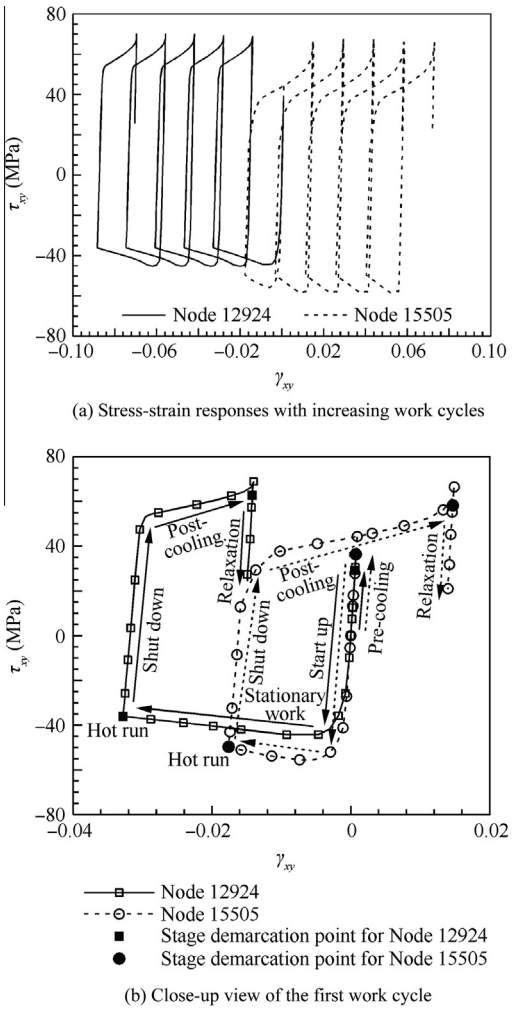

Fig. 9 Shear stress–strain curves of typical nodes during cyclic work process.

4.3. Low-cycle fatigue damage and life estimation

In accordance with the thermal-structural response during the cyclic working process, the obtained low-cycle fatigue damage distributions of channel wall nozzle are presented in Fig. 10(a). It is apparent that the perceptible fatigue damage mainly occurs in the front region of the slotted liner. The increasing nozzle work cycles bring about remarkable fatigue damage accumulation, especially obvious in the intersecting dangerous areas of liner gas side wall and symmetric planes of channel and rib. As similar thermo-mechanical behavior of channel wall nozzle has been acquired in each work cycle, the low-cycle fatigue life distribution applying Miner's rule of linear damage accumulation on the basis of the calculated fatigue damage in the first work cycle is given in Fig. 10(b). Obviously, the estimated service life has the uniform distribution feature with the fatigue damage. The fatigue lives of the typical Node 12924 and Node 15505 equal to 112.8 and 117.5 cycles respectively.

Fig. 11 has provided the evaluated low-cycle fatigue damage values of the representative nodes with increasing nozzle work cycles. Although the computed strain amplitudes as well as the residual strain increments of the typical nodes in each work cycle are almost equal, the fatigue damages of the two nodes accumulate nonlinearly. A simplified nonlinear damage accumulation method is proposed to estimate the low-cycle fatigue life of channel wall nozzle. It applies a fitted quadratic polynomial curve with the formula as in Eq. (10) according to the obtained node damage amassing trend. The dependency relationship between the nonlinear prediction damage D_{non} and the number of nozzle work cycles N is defined by the

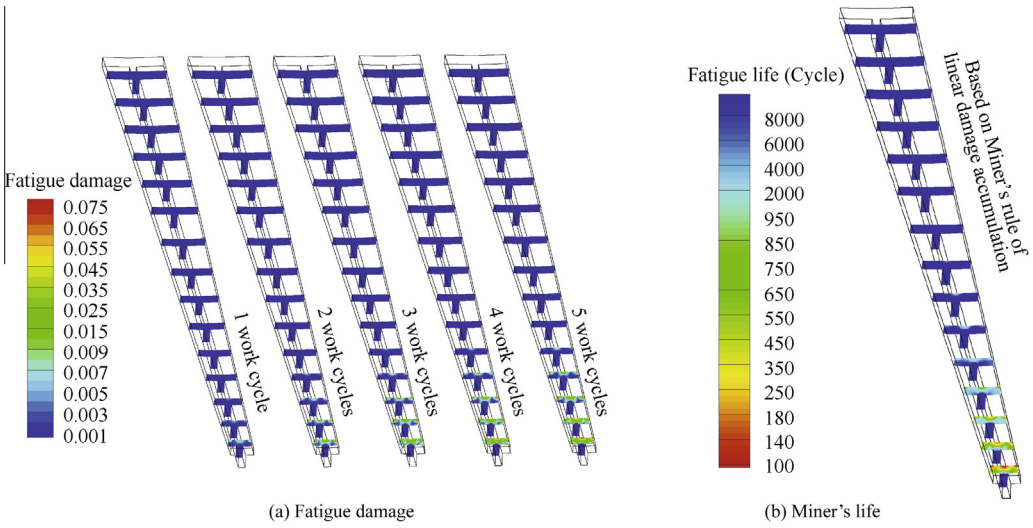

Fig. 10 Low-cycle fatigue damage and Miner's life distributions of channel wall nozzle.

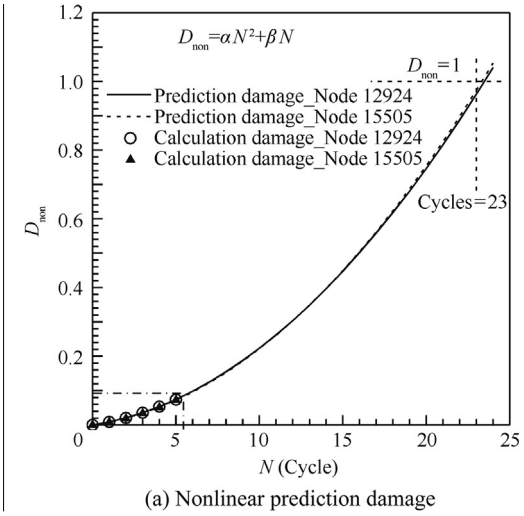

(a) Nonlinear prediction damage

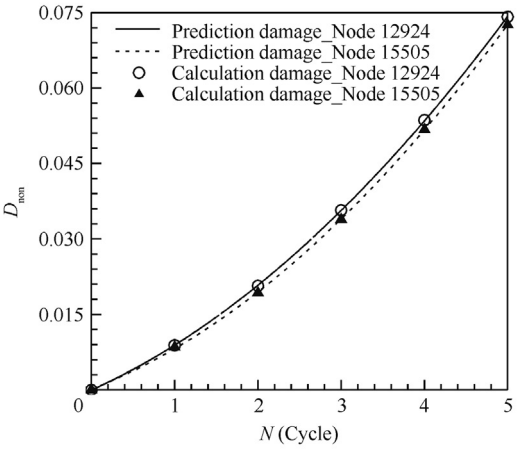

(b) Partial enlarged detail of Fig. 11(a)

Fig. 11 Node low-cycle fatigue damage during cyclic work process.

coefficient α and β, both of which are determined by the strain history of the specified node. The nonlinearly predicted low-cycle fatigue damages of Node 12924 and Node 15505 with increasing work cycles are described in Fig. 11. It indicates that the service lives of the two nodes are 23 missions, which are the relatively conservative estimation far below the Miner's lives. In practice, the low-cycle fatigue life of channel wall nozzle can be assessed by the measured damage accumulation trend lines in crucial locations of test model, which is chosen randomly from a batch of identical reusable nozzles.

$$D_{\text{non}} = \alpha N^2 + \beta N \tag{10}$$

5. Conclusions

(1) During the cyclic work of channel wall nozzle, the variation of non-uniform thermal load distribution plays a significant role in the thermal-structural response by altering the material properties.

(2) The interaction of thermal–mechanical loads and varying material strength during the cyclic work results in serious strain in the front region of the slotted liner. The most dangerous areas of channel wall nozzle are located at the intersecting regions of the liner gas side wall and symmetric planes of channel and rib. With the increase in nozzle work cycle, the residual strain accumulates linearly, and the strain amplitudes as well as the increments in each work cycle are almost equal respectively.

(3) The most serious fatigue damage occurs in the critical locations of slotted liner, where the fatigue failure takes place initially. To estimate the nonlinearly growing up fatigue damage of channel wall nozzle, a simplified nonlinear damage accumulation approach has been proposed. The predicted lives of the typical nodes are obviously conservative to the Miner's lives.

(4) To improve the durability of channel wall nozzle, several ways have been suggested, including appropriately attenuating the liner thickness at nozzle inlet but increasing it at nozzle outlet, applying multi-section cooling concept and employing coolant forward flow layout etc.

References

1. Sackheim RL. Overview of United States space propulsion technology and associated space transportation systems. *J Propul Power* 2006;**22**(6):1310–33.
2. Jones D. *Reusable rocket propulsion for space tourism vehicles*; 2004. Report No.: AIAA-2004-3742.
3. Van Hooser KP, Bradley DP. *Space shuttle main engine — the relentless pursuit of improvement*; 2011. Report No.: AIAA-2011-7159.
4. Gradl PR, Stephens W. *Space shuttle main engine debris testing methodology and impact tolerances*; 2005. Report No.: AIAA-2005-3628.
5. Sutton GP. History of liquid-propellant rocket engines in Russia, formerly the Soviet Union. *J Propul Power* 2003;**19**(6):1008–37.
6. Fint J, Kuck F, Sciorelli F. *Development of channel wall nozzles for use on liquid propellant rocket engine*; 2005. Report No.: AIAA-2005-4306.
7. Miller RW. *Low-cycle fatigue analysis of a cooled copper combustion chamber*; 1974. Report No.: AIAA-1974-1079.
8. Desmorat B, Desmorat R. *Topology optimization of elasto-plastic structures in damage governed low cycle fatigue*; 2007. Report No.: AIAA-2007-1925.
9. Naeem M. Implications of day temperature for a high-pressure-turbine blade's low-cycle-fatigue life consumption. *J Propul Power* 2008;**24**(3):624–8.
10. Porowski JS, O'Donnell WJ, Badlani ML, Kasraie B, Kasper HJ. Simplified design and life prediction of rocket thrust chambers. *J Spacecr Technol* 1985;**22**(2):181–7.
11. Dai XW, Ray A. Life prediction of the thrust chamber wall of a reusable rocket engine. *J Propul Power* 1995;**11**(6):1279–87.
12. Sung IK, Anderson W. *A Subscale-based rocket combustor life prediction methodology*; 2005. Report No.: AIAA-2005-3570.
13. Riccius JR. *Cyclic laser heating and optical measurement of combustion chamber wall structures;* 2012. Report No.: AIAA-2012-4011.
14. Pizzarelli M, Nasuti F, Paciorri R, Onofri M. Numerical analysis of three-dimensional flow of supercritical fluid in asymmetrically heated channels. *AIAA J* 2009;**47**(11):2534–43.
15. Pizzarelli M, Nasuti F, Onofri M. *CFD analysis of curved cooling channel flow and heat transfer in rocket engines*; 2010. Report No.: AIAA-2010-6722.
16. Boman A, Haggander J. *Laser welded channel wall nozzle design, manufacturing and hot gas testing*; 1999. Report No.:AIAA-1999-2750.
17. Winterfeldt L, Stenstrom E. *Functional aspects on laser welded sandwich walls for rocket engine nozzles*; 2001. Report No.:AIAA-2001-3695.
18. Ellis DL, Michal GM. *Mechanical and thermal properties of two Cu–Cr–Nb alloys and NARloy-Z*; 1985. Report No.: NASA-CR-198529.
19. Kim JW, Lee DJ. Characteristic interface conditions for multi-block high-order computation on singular structured grid. *AIAA J* 2003;**41**(12):2341–8.
20. Amsallem D, Farhat C. Interpolation method for adapting reduced-order models and application to aeroelasticity. *AIAA J* 2008;**46**(7):1803–13.
21. Riccius JR, Haidn OJ, Zametaev EB. *Influence of time dependent effects on the estimated life time of liquid rocket combustion chamber walls*; 2004. Report No.: AIAA-2004-3670.
22. Arya VK, Arnold SM. Viscoplastic analysis of an experimental cylindrical thrust chamber liner. *AIAA J* 1992;**30**(3):781–9.
23. Riccius JR, Hilsenbeck MR, Haidn OJ. *Optimization of geometric parameters of cryogenic liquid rocket combustion chambers*; 2001. Report No.: AIAA-2001-3408.
24. Kalev I. Cyclic plasticity and fatigue of structural components. *J Aircraft* 1981;**18**(10):869–73.
25. Sung IK. *Fatigue life prediction of liquid rocket engine combustor with subscale test verification.* West Lafayette: Purdue University; 2006.
26. Weiss JM, Smith WA. Preconditioning applied to variable and constant density flows. *AIAA J* 1995;**33**(11):2050–7.
27. Choi Y, Merkle CL. *Time-derivative preconditioning for viscous flows*; 1991. Report No.: AIAA-91-1652.
28. Bauer M, Dierke J, Ewert R. Application of a discontinuous Galerkin method to discretize acoustic perturbation equations. *AIAA J* 2011;**49**(5):898–908.
29. Amar AJ, Blackwell BF, Edwards JR. One-dimensional ablation using a full Newton's Method and finite control volume procedure. *J Thermophys Heat Tr* 2008;**22**(1):71–82.
30. Zhang XG, Liu Y, Ren JX, Zhan K. *Nonlinear finite element analysis of the SRM flexible joint*; 2012. Report No.: AIAA-2012-1453.
31. Kuhl D, Riccius J, Haidn OJ. Thermomechanical analysis and optimization of cryogenic liquid rocket engines. *J Propul Power* 2002;**18**(4):835–46.
32. Esposito JJ, Zabora RF. *Thrust chamber life prediction: Volume 1, mechanical and physical properties of high performance rocket nozzle materials*; 1975. Report No.: NASA-CR-134806.
33. Basquin OH. *The exponential law of endurance tests.* West Conshohocken: American Society for Testing and Materials; 1910.
34. Gyllenskog J, Ladani LJ. Fatigue crack initiation and propagation in aileron lever using successive-initiation modeling approach]. *J Aircraft* 2011;**48**(4):1387–95.
35. Miner MA. Cumulative damage in fatigue. *J Appl Mech* 1945;**6**(7):159–64.
36. Halford GR, Nachtigall AJ. Strainrange partitioning behavior of an advanced gas turbine disk alloy AF2-1DA. *J Aircraft* 1980;**17**(8):598–604.
37. Dowling NE. Fatigue life prediction for complex load versus time histories. *J Eng Mater Tech* 1983;**105**:206–14.
38. Manson SS, Halford G. *A method of estimating high temperature low cycle fatigue behavior of materials*; 1967. Report No.: NASA TMX-52270.
39. Ray A, Dai XW, Wu MK, Carpino M, Lorenzo CF. Damage-mitigating control of a reusable rocket engine. *J Propul Power* 1994;**10**(2):225–34.

Cheng Cheng is a Ph.D. student at School of Astronautics, Beihang University. His main research interest is the reusable rocket propulsion technology.

Wang Yibai is a associate professor at School of Astronautics, Beihang University. His main research interest is the aerospike nozzle technology.

Liu Yu is a renowned professor at School of Astronautics, Beihang University. His main research interest is the new concept of the rocket propulsion technology.

Liu Dawei is a graduate student at School of Astronautics, Beihang University. His main research interest is the cold test of reusable channel wall nozzle.

Lu Xingyu is a graduate student at School of Astronautics, Beihang University. His main research interest is the cold test of nozzle side load.